Behaviors of Class-F and Class-F^{-1} Amplifiers

Junghwan Moon, *Student Member, IEEE*, Seunghoon Jee, *Student Member, IEEE*, Jungjoon Kim, *Student Member, IEEE*, Jangheon Kim, *Member, IEEE*, and Bumman Kim, *Fellow, IEEE*

***Abstract*—Operational behaviors of the class-F and class-F^{-1} amplifiers are investigated. For the half-sinusoidal voltage waveform of the class-F^{-1} amplifier, the amplifier should be operated in the highly saturated region, in which the phase relation between the fundamental and second harmonic currents are out-of-phase. The class-F amplifier can operate at the less saturated region to form a half sinewave current waveform. Therefore, the class-F^{-1} amplifier has a bifurcated current waveform from the hard saturated operation, but the class-F amplifier operates as a switch at the saturated region for a second harmonic tuned half-sine waveform. To get the hard saturated operation, the fundamental load is very large, more than $\sqrt{2}$ times larger than that of the tuned load amplifier. The operational behaviors of the amplifiers are explored with the nonlinear output capacitor. Since the capacitor generates a large second harmonic voltage with smaller higher order terms, the class-F^{-1} amplifier with the nonlinear capacitor can deliver the proper half-sinusoidal voltage waveforms at a lower power, but the effect of the nonlinear capacitor is small for the class-F amplifier. The class-F^{-1} amplifier delivers the superior performance at the highly saturated operation due to its larger fundamental current and voltage generation at the expense of the larger voltage swing. The simulation results lead to the conclusion that the class-F^{-1} amplifier with the nonlinear capacitor is suitable topology for high efficiency. However, in the strict sense, the class-F^{-1} amplifier with the nonlinear capacitor is not the classical class-F^{-1} amplifier because the voltage-shaping mechanisms and the fundamental load are quite different. We call it the saturated amplifier since the amplifier is the optimized structure of the power amplifier operation at the saturated mode.**

***Index Terms*—Class-F^{-1}, class-F, efficiency, nonlinear capacitor, power amplifier (PA), saturated PA.**

I. Introduction

HIGH efficiency is a crucial design consideration not only for the power amplifier (PA) itself, but also for the transmitters, such as Doherty and supply modulated PAs, for thermal management, reliability, and size [1]–[23]. Several PA topologies, such as class-E, class-F, and class-F^{-1}, have been proposed to achieve high efficiency [3]–[17]. In the class-E PA, a transistor acts as a switch. The voltage of the class-E amplifier is generated by charging and discharging of output capacitor in parallel with the switch. Since this amplifier tunes all harmonic components using the *LC* resonator, it delivers the highest efficiency among the proposed amplifiers. However, the charging step of the capacitor cannot be abrupt. Above the theoretical maximum frequency $f_{\max,E}$, the capacitor cannot discharge fast enough to support the ideal waveform [3], [4]. As a result, efficiency of the class-E PA is degraded significantly at the high frequency above $f_{\max,E}$ [3]–[6].

To deliver high efficiency at the high frequency, the harmonically tuned PAs, such as class-F and class-F^{-1} amplifiers, have been extensively studied [7]–[23]. The ideal class-F amplifier has half-sinusoidal current and rectangular voltage waveforms in conjunction with the short circuit for even harmonic and open circuit for odd harmonic. Thus, there is no overlapping between the current and voltage, resulting in zero internal dissipation power. In addition, since there is no harmonic power, the class-F amplifier delivers the theoretical efficiency of 100%. The class-F^{-1} is a dual of the class-F PA where the current and voltage waveforms are interchanged. With the same drain supply voltage, the class-F^{-1} amplifier has larger peak voltage value than that of class-F, incurring the reliability problem due to breakdown of the device. Thus, some research has compared and analyzed the class-F and class-F^{-1} PAs under the condition of the same voltage swing [7], [8]. Recently, due to advances in wide bandgap semiconductor technology such as gallium–nitride (GaN) high electron-mobility transistor (HEMT) technology, a large voltage swing becomes feasible. This resolves the maximum voltage limitation of the class-F^{-1} amplifier, allowing the amplifier to operate with the same supply voltage of the class-F PA. As the breakdown issue of the class-F^{-1} amplifier is moderated, a lot of research has investigated the PAs under the condition of the same supply voltage [9]–[16]. Although the previous research clearly show that the class-F^{-1} amplifier outperforms the class-F PA, there is no in-depth explanation for the performance of the class-F^{-1} amplifier. Moreover, most of these analyses have been carried out under the assumption of the linear input and output device capacitances.

In this paper, the class-F and class-F^{-1} amplifiers are numerically compared in terms of the optimum load impedance, output power, and efficiency according to the conduction angle. The numerical analysis is validated using a simplified model with linear and nonlinear capacitors. Unlike the class-F amplifier, the operation of the class-F^{-1} PA is strongly affected by the nonlinear output capacitor because the capacitor generates a

Manuscript received October 01, 2011; revised February 07, 2012; accepted February 21, 2012. Date of publication April 06, 2012; date of current version May 25, 2012. This work was supported by The Ministry of Knowledge Economy (MKE), Korea, under the Information Technology Research Center (ITRC) support program supervised by the National IT Industry Promotion Agency (NIPA) [NIPA-2012-(C1090-1211-0011)], the World Class University program funded by the Ministry of Education, Science and Technology through the National Research Foundation of Korea (R31-10100), and the Brain Korea 21 Project in 2012.

J. Moon is with the Department of Electrical Engineering and the Division of Information Technology Convergence Engineering, Pohang University of Science and Technology, Pohang, Gyeongbuk, 790-784, Korea, and also with the Telecommunication Systems Division, Samsung Electronics Company Ltd., Suwon, Gyeunggi 443-742, Korea (e-mail: jhmoon@postech.ac.kr).

S. Jee, J. Kim, and B. Kim are with the Department of Electrical Engineering and Division of Information Technology Convergence Engineering, Pohang University of Science and Technology, Pohang, Gyeongbuk, 790-784, Korea (e-mail: cshcomit@postech.ac.kr; jungjoon@postech.ac.kr; bmkim@postech.ac.kr).

J. Kim is with the Telecommunication Systems Division, Samsung Electronics Company Ltd., Suwon, Gyeunggi 443-742, Korea (e-mail: jangheon.kim@samsung.com).

Digital Object Identifier 10.1109/TMTT.2012.2190749

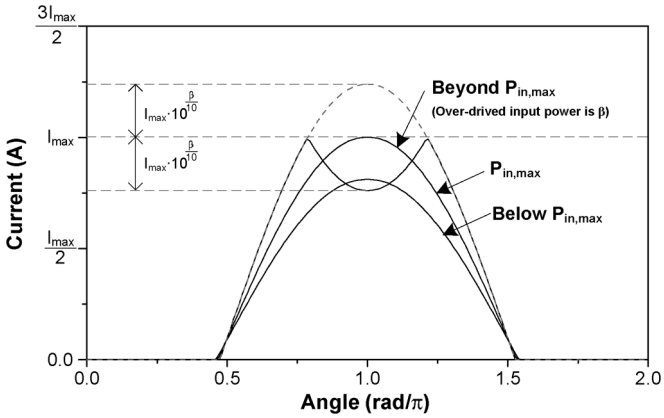

Fig. 1. Modeled current waveform when the PA is overdriven.

large second harmonic voltage component, shaping the voltage waveform. The current waveform is bifurcated due to the saturated operation, resulting in a quasi-rectangular waveform [15], [21]. The operation of class-F amplifier is different and the bifurcation does not occur. Thus, the fundamental current of the class-F^{-1} PA is reduced and voltage is enlarged, requiring a large fundamental load. The fundamental load should be $\sqrt{2}$ times larger than that of the tuned amplifier. Thus, the class-F^{-1} PA with the nonlinear capacitor can be considered a new kind of amplifier, which is called as a saturated amplifier [3], [19]–[21]. This amplifier is the optimized structure of PA operation at the saturated mode. Although the current and voltage waveforms of the saturated amplifier are the same as those of the class-F^{-1} amplifier, the waveform-shaping mechanisms of both amplifiers are different.

This paper is organized as follows. In Section II, the class-F and class-F^{-1} amplifiers are numerically analyzed according to the conduction angle. In addition, the numerical analysis is verified by the simplified device model with the linear capacitor. With the device model with the nonlinear capacitor, the operational behaviors of the both amplifiers are further explored in Section III. In Section IV, the commercial device model is used for comparing the class-F and saturated amplifiers. In addition, the operation of the saturated amplifier using the model is verified. Finally, the conclusions are presented in Section V.

II. Analysis for Basic Operation of Class-F and Class-F^{-1} Amplifiers Using Idealized Current Waveform

In this section, the class-F and class-F^{-1} amplifiers are analyzed for output power, efficiency, and gain performances in terms of input overdriving power, load impedance, and conduction angle. Numerical analysis is carried out using an idealized current waveform, shown in Fig. 1, then a simplified device model is employed to validate the analysis. The following analysis and results are dependent on harmonic load such as operation at the saturation region. The process is accurate for the class-F^{-1} amplifier, but has a limitation for the class-F amplifier. However, the class-F amplifier does not drive into the saturated mode. Thus, the followings provide the operation behaviors and good guidelines for the class-F and class-F^{-1} amplifiers.

A. Numerical Comparison

1) Basic Formulations: For the numerical analysis of the class-F and class-F^{-1} amplifiers, most of assumptions, related to the active device, the number of harmonics to be controlled, and the load conditions, are made based on [15], [17], and [18]. The additional assumptions used in this study are as follows.

- Input harmonic is not considered, and the current waveform is assumed to be bifurcated when the amplifier is overdriven beyond the maximum linear input power level, as shown in Fig. 1, where β is the overdriving ratio.
- The same supply voltages are assumed for both amplifiers.

Based on the assumptions, the voltage waveforms of the class-F and class-F^{-1} PAs [17], [18] are expressed by

$$V_{\mathrm{F}}(\theta) = V_{\mathrm{DC}} - \delta(k_3) \cdot [V_{1,\mathrm{TL}} \cdot \cos(\theta) - k_3 \cdot V_{1,\mathrm{TL}} \cdot \cos(3\theta)] \quad (1)$$

$$V_{\mathrm{F}^{-1}}(\theta) = V_{\mathrm{DC}} - \delta(k_2) \cdot [V_{1,\mathrm{TL}} \cdot \cos(\theta) - k_2 \cdot V_{1,\mathrm{TL}} \cdot \cos(2\theta)]\,. \quad (2)$$

$\delta(k_2)$, $\delta(k_3)$, k_2, and k_3 are defined by

$$\delta(k_2) \equiv \frac{V_{1,\mathrm{F}^{-1}}}{V_{1,\mathrm{TL}}} \quad \delta(k_3) \equiv \frac{V_{1,\mathrm{F}}}{V_{1,\mathrm{TL}}}$$
$$k_2 \equiv \frac{V_{2,\mathrm{F}^{-1}}}{V_{1,\mathrm{F}^{-1}}} \quad k_3 \equiv \frac{V_{3,\mathrm{F}}}{V_{1,\mathrm{F}}}. \quad (3)$$

For the class-F amplifier, the maximum fundamental voltage, which is $\delta(k_3) = 1.15$ times larger than that of the tuned load amplifier ($V_{1,\mathrm{TL}}$), can be achieved with k_3 of 1/6 [17]. The tuned load amplifier represents the amplifier with short-circuit termination for all harmonics. Similarly, for the class-F^{-1} amplifier, the maximum fundamental voltage, $\delta(k_2) = \sqrt{2}$ times larger than that of the tuned load PA, can be obtained with k_2 of $\sqrt{2}/4$ [18]. For the resistive loads, the amplifiers can have the maximum fundamental voltages when the phase relation between the fundamental and each harmonic component are out-of-phase. However, as shown in Fig. 2, the phase relation between the fundamental and second or third harmonic is not always satisfied, and can be achieved only at the overdriven operation.

Since the active device acts as an ideal voltage controlled current source, the proper voltage waveforms for the class-F and class-F^{-1} amplifiers can be obtained using the suitable load impedances. The required third harmonic load impedance for the class-F amplifier and second harmonic load impedance for the class-F^{-1} amplifier are derived from k_3 and k_2, respectively [17], [18]. The harmonic load impedances are proportional to the current ratios. However, the harmonic current components are quite small compared to the fundamental current when the phases of the harmonic components begin to reverse from in-phase to out-of-phase, as shown in Fig. 2. As a result, the required harmonic load impedances are very large and unfeasible. For practical comparison, the performances of the

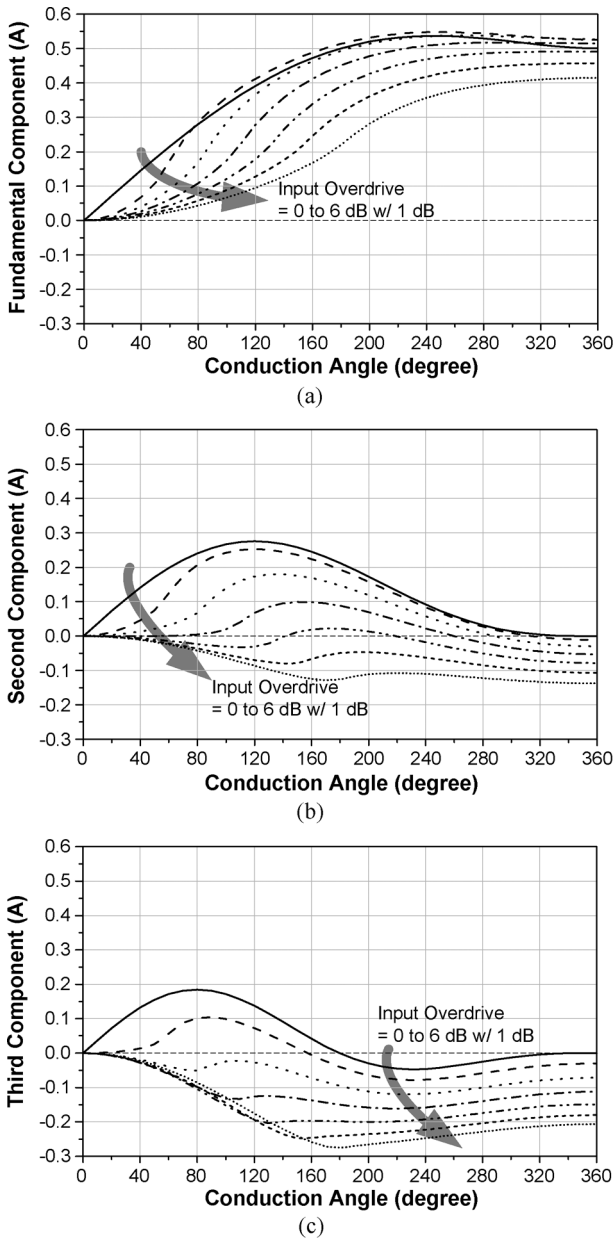

Fig. 2. Fourier components of the overdriven current waveform shown in Fig. 1. (a) Fundamental, (b) second harmonic, and (c) third harmonic components.

class-F and class-F^{-1} amplifiers are compared under the condition that the required third or second harmonic load impedance is less than five times the fundamental load impedance. The required input overdrive ratios, according to the conduction angle, for the class-F and class-F^{-1} amplifiers are depicted in Fig. 3. Compared to the class-F, the class-F^{-1} amplifier requires larger overdrive ratio, reducing the fundamental current as shown in Fig. 2(a). In this figure, the practical case represents when the required harmonic load impedances are limited to the five times of the fundamental load impedances and ideal case represents when the harmonic load impedances are not limited.

2) Comparison: Fig. 4 shows the calculated fundamental load impedance ratios for the class-F and class-F^{-1} PAs over the tuned load amplifier. For conduction angle above 120°, the

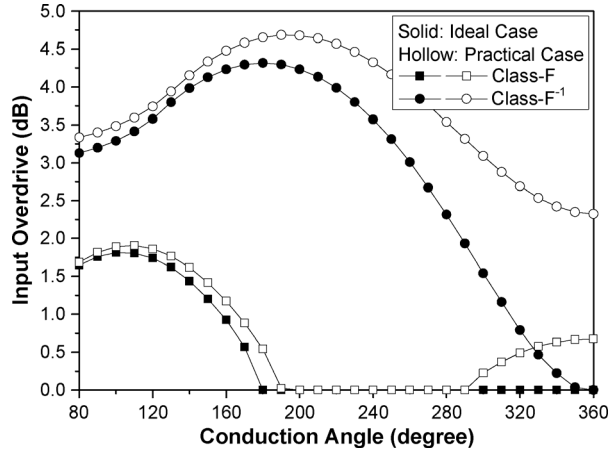

Fig. 3. Calculated input overdrive ratios to achieve the proper operations of class-F and class-F^{-1} amplifiers.

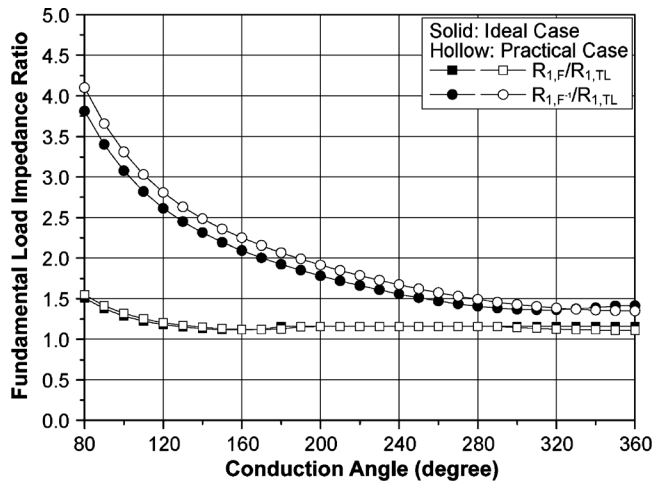

Fig. 4. Calculated fundamental load impedance ratios for class-F and class-F^{-1} amplifiers with respect to the tuned load PA.

class-F PA has the fundamental voltage 1.15 times larger than that of the tuned load PA, while the fundamental current is similar to that of the tuned load PA because the required phase relation can be satisfied with low input overdrive level less than 2 dB. For this level, the fundamental current is nearly maintained for the maximum value, as shown in Fig. 2(a), for the conduction angle above 120°. However, for the conduction angle below 120°, the fundamental load impedance starts to increase, but the conduction angle below 120° is not usually employed because of the low output power. Thus, the fundamental load impedance of the class-F amplifier $R_{\mathrm{opt,F}}$ can be regarded as $1.15 \cdot R_{\mathrm{opt,TL}}$. The class-F^{-1} amplifier delivers the fundamental voltage $\sqrt{2}$ times larger than that of the tuned load amplifier. However, it requires the highly overdriven operation to obtain the proper phase relation, as shown in Fig. 3. As a result, the fundamental current of the class-F^{-1} amplifier is lower than that of the class-F or tuned load amplifiers for most of the conduction angles. Although the ideal fundamental load impedance ratio of the class-F^{-1} PA is about $\sqrt{2}$, the impedance increases significantly as the conduction angle decreases. It is worthwhile to notice that the bifurcated current waveform is suitable to the

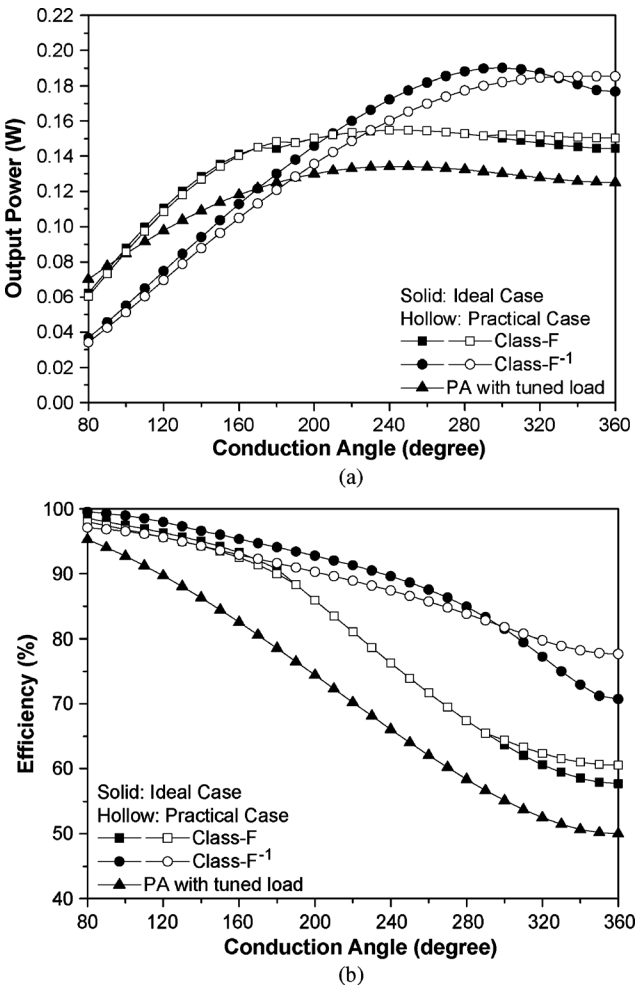

Fig. 5. Calculated output performances of class-F, class-F^{-1}, and tuned load PAs. (a) Output power. (b) Efficiency.

class-F^{-1} amplifier, but not to the class-F amplifier. However, the class-F amplifier operates near the saturation region and the error can be small. Also, this model does not accurately describe the saturated characteristic of the current, and we will revisit this behavior in Section II-B.2.

Fig. 5 shows the calculated output power and efficiency characteristics of the class-F, class-F^{-1}, and tuned load amplifiers. Due to the reduced fundamental current of the class-F^{-1} amplifier, this amplifier delivers the output power less than that of the class-F or tuned load PA below the conduction angle of 220° even though the class-F^{-1} amplifier has the largest fundamental voltage component. As the conduction angle increases, the required input overdrive ratio decreases and the fundamental current of the class-F^{-1} amplifier increases rapidly, resulting in the larger output power, as shown in Fig. 5(a).

Fig. 5(b) illustrates the efficiencies of the amplifiers. Since the class-F^{-1} amplifier operates at a highly saturated mode for all conduction angles, the ratio of fundamental to dc currents of the amplifier is lower than that of the class-F or tuned load PA. However, among the three PAs, the class-F^{-1} PA has the largest fundamental voltage component for the same dc bias. Thus, at the low conduction angle below 180°, the current is low and the efficiency is similar to that of the class-F amplifier. As the conduction angle increases, the class-F^{-1} amplifier is still in the heavily saturated region, but the fundamental current increases, and the ratio of fundamental to dc currents increases, enhancing the efficiency, as shown in Fig. 5(b).

B. Analysis Using Simplified Device Model

In this section, the numerical analysis carried out in Section II-A is verified using the simplified device model with a linear capacitor. The comparison is made for the conduction angle between 180° and 250°, which is the practical operation region.

1) Device Model: Fig. 6(a) shows the simplified transistor model employed in this study. It consists of the input capacitor $C_{\rm IN}$, input resistance $R_{\rm IN}$, nonlinear voltage-controlled current source, nonlinear output conductance $g_{\rm ds}$, and output capacitor $C_{\rm OUT}$. The feedback capacitor is absorbed into $C_{\rm IN}$ and $C_{\rm OUT}$ by the Miller theorem. Fig. 6(b) depicts the dc–*IV* characteristic, extracted from Cree GaN HEMT CGH60015 large-signal model by applying the pulsed signal. The extracted input and output capacitors are illustrated in Fig. 6(c) and (d), respectively. Although the capacitors are nonlinear, they are regarded as the linear components to simply explore the operation of the class-F and class-F^{-1} amplifiers. However, in Section III, the transistor model including the nonlinear capacitors is employed to accurately investigate the operational behaviors of the amplifiers.

2) Results: For reference, a tuned load PA is also designed during the analysis of class-F and class-F^{-1} amplifiers. In order to maximize the gain, the fundamental source impedances for all PAs are conjugately matched to $3 + j17.1\ \Omega$, while the harmonics at the input are shorted. The fundamental load impedance of the tuned load PA is determined by

$$R_{\rm opt,TL} = \frac{V_{\rm DC} - V_k}{I_1(\alpha)}. \tag{4}$$

α corresponds to the conduction angle. During the simulation, all amplifiers have the drain supply voltage of 30 V. Since the class-F amplifier has 1.15 times larger fundamental voltage and the comparable fundamental current compared to the tuned load PA, $R_{\rm opt,F}$ is $1.15 \cdot R_{\rm opt,TL}$, as mentioned in Section II-A.2. Although the class-F^{-1} amplifier delivers $\sqrt{2}$ times larger fundamental voltage than the tuned load PA, the amplifier operates in deeply saturated region, in which the fundamental current cannot be exactly estimated. Thus, the fundamental load impedance of the class-F^{-1} amplifier is optimized for the maximum output power. The harmonic manipulation at the load is carried out up to third harmonic for simplicity. For the tuned load PA, the harmonics at the load are shorted. For the class-F amplifier, the second harmonic is shorted, but the third harmonic is selected to maximize output power and efficiency, but is limited to five times $R_{\rm opt,F}$. Similarly, the third harmonic of the class-F^{-1} amplifier is shorted, but the second harmonic of the amplifier is optimized for the output power and efficiency within five times $R_{\rm opt,F^{-1}}$.

Since the current model used in Section II-A is an idealized one, the fundamental current at the deeply saturated region is much lower than that of the real device model. Thus, the impedance ratio of the class-F amplifier is similar to the real

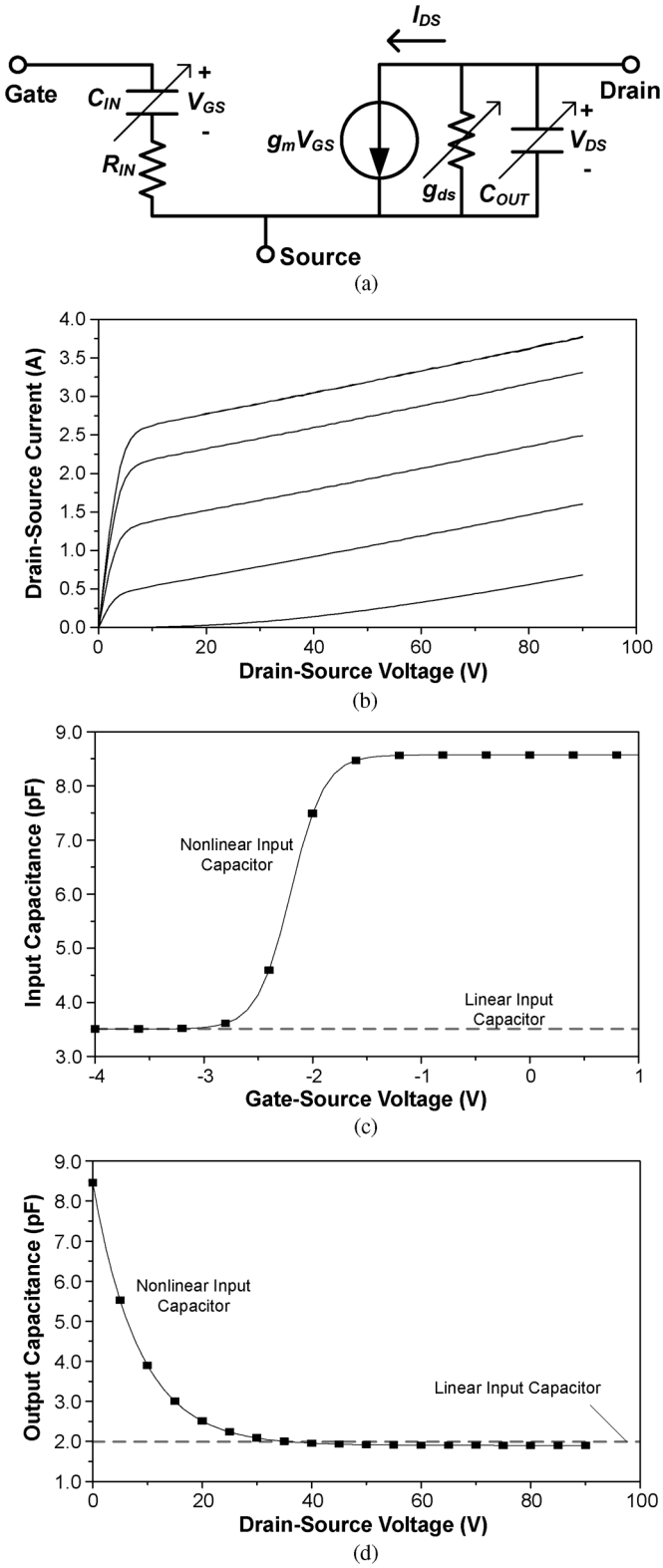

Fig. 6. Simplified transistor model used in this study. (a) Equivalent transistor model. (b) DC–*IV* characteristic. Capacitances for the linear and nonlinear: (c) input capacitors and (d) output capacitors. All parameters in (a) are extracted from the Cree GaN HEMT CGH60015 large-signal model using Agilent ADS.

case, but that of the class-F^{-1} amplifier is somewhat exaggerated. The impedance of the class-F^{-1} amplifier is almost constant for the conduction angle. Fig. 7 shows the simulated load impedance ratios of the class-F and class-F^{-1} amplifiers. This

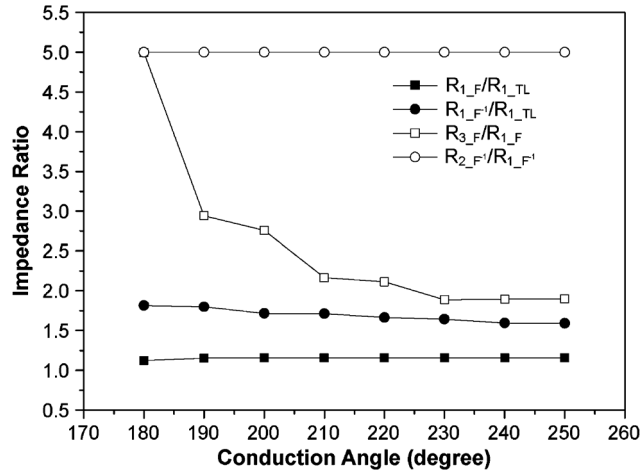

Fig. 7. Simulated load impedance ratios.

larger voltage of the class-F^{-1} amplifier increases the output power of the amplifier, and even at a low conduction angle, the output powers of the class-F and class-F^{-1} PAs are similar, as shown in Fig. 8(a). Due to the heavily saturated operation of the class-F^{-1} amplifier, the gain is lower than that of the class-F or tuned load PA, as shown in Fig. 8(b). As mentioned in Section II-A.2, the fundamental voltages of the amplifiers are nearly the same for the different conduction angle. The maximum voltages of the amplifiers are nearly maintained, 76.5 V for the class-F^{-1} amplifier and 57.2 V for the class-F and tuned load PAs. The ratio of the fundamental current to dc current of the class-F^{-1} amplifier is nearly constant for the larger conduction angle, as shown in Fig. 9, and the efficiency of the class-F^{-1} amplifier is maintained at the larger conduction angle, while those of the other PAs are reduced, as shown in Fig. 8(b). In addition, the fundamental load impedance of the class-F^{-1} amplifier is larger than that of the class-F amplifier, and the class-F^{-1} amplifier has a reduced knee voltage effect, increasing the efficiency. Thus, the efficiency difference between the two amplifiers is slightly increased compared to the difference in Fig. 5(b).

In short, the simulation based on the idealized current waveform is accurate, except for the class-F^{-1} amplifier with a small conduction angle. The model predicts that as the conduction angle increases, the class-F^{-1} amplifier is superior to the class-F PA for the output power and efficiency. However, for the proper voltage shaping of the class-F^{-1} amplifier, it should be driven into the deeply saturated state, degrading the power gain and requiring a large voltage swing.

III. Power-Level-Dependent Characteristics of Class-F and Class-F^{-1} Amplifiers Using the Simplified Model

In this section, the operational behaviors of the class-F and class-F^{-1} amplifiers are further investigated with the device model, including the input and output nonlinear capacitors, as shown in Fig. 6. These capacitors vary according to the power level. Thus, the comparison of the class-F and class-F^{-1} amplifiers are accomplished according to the power level. Although the class-B or class-C biased PA delivers better efficiency, it has poor linearity with lower output power compared to the class-AB amplifier. Thus, hereafter, all PAs are biased at the

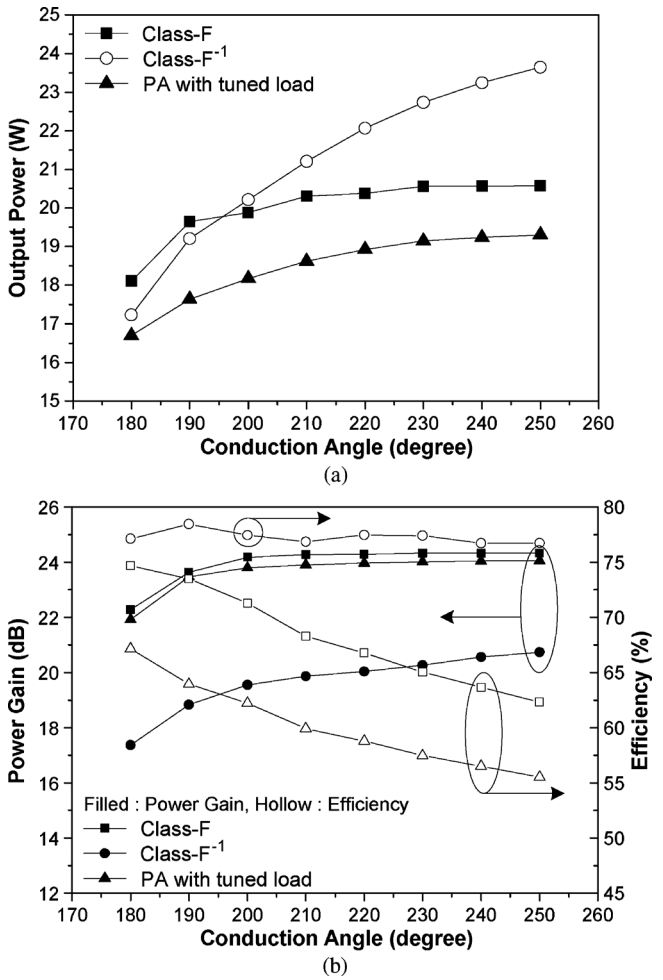

Fig. 8. Simulated performances of class-F, class-F^{-1}, and tuned load PAs versus conduction angle. (a) Output power. (b) Power gain and efficiency.

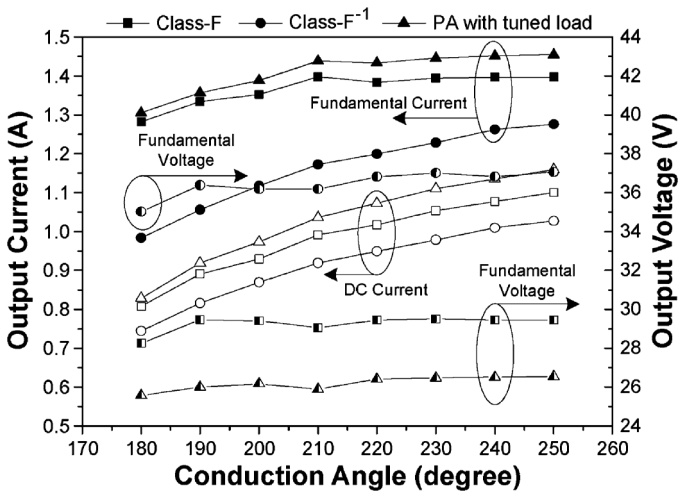

Fig. 9. Simulated output currents and voltages of class-F, class-F^{-1}, and tuned load PAs.

class-AB PA with a conduction angle of 190°. The optimum load impedances for the amplifiers are initially selected based on the analysis in Section II, then slightly tuned to maximize the output power and efficiency.

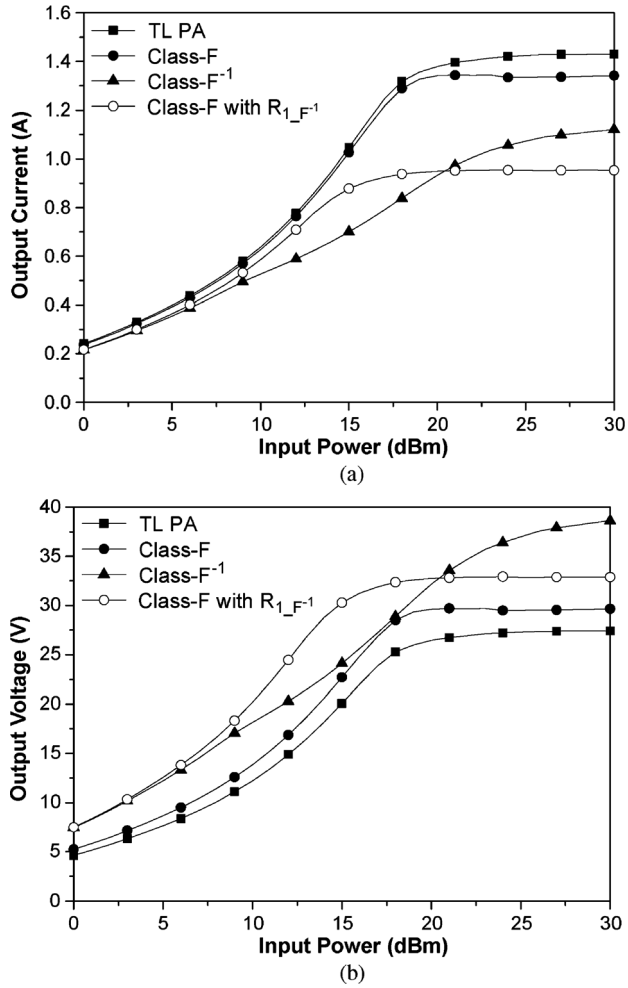

Fig. 10. Simulated fundamental: (a) output currents and (b) voltages of class-F, class-F with the $R_{\mathrm{opt},\mathrm{F}^{-1}}$, class-$F^{-1}$, and tuned load PAs according to the input power level. During the simulation, all PAs are biased at a conduction angle of 190°.

A. Class-F and Class-F^{-1} Amplifiers with Linear Capacitor

Before considering the effects caused by the nonlinear capacitor, for a reference, the power-level dependent behaviors of the class-F and class-F^{-1} amplifiers with the linear capacitor are analyzed. To compare the amplifiers under the same knee voltage effect, the class-F amplifier with $R_{\mathrm{opt},\mathrm{F}^{-1}}$ is also designed. Fig. 10 shows the simulated fundamental currents and voltages of the class-F, class-F with the $R_{\mathrm{opt},\mathrm{F}^{-1}}$, class-$F^{-1}$, and tuned load amplifiers, and Fig. 11 depicts the simulated voltage and current waveforms and load-lines of the amplifiers. For the input power of below 10 dBm, all PAs are in the linear region, in which the current is mainly determined by the input power. Thus, the fundamental currents of the PAs are nearly the same at the region. However, since the class-F^{-1} and class-F amplifiers with the $R_{\mathrm{opt},\mathrm{F}^{-1}}$ amplifiers have a fundamental load impedance larger than the other PAs, their maximum currents are limited. Compared to the class-F amplifier, the fundamental voltages of the other two amplifiers are larger due to the larger fundamental load.

As the input power increases, the amplifiers generate harmonic currents, shaping the voltage waveforms. Since the phase relation of the fundamental to third harmonic currents

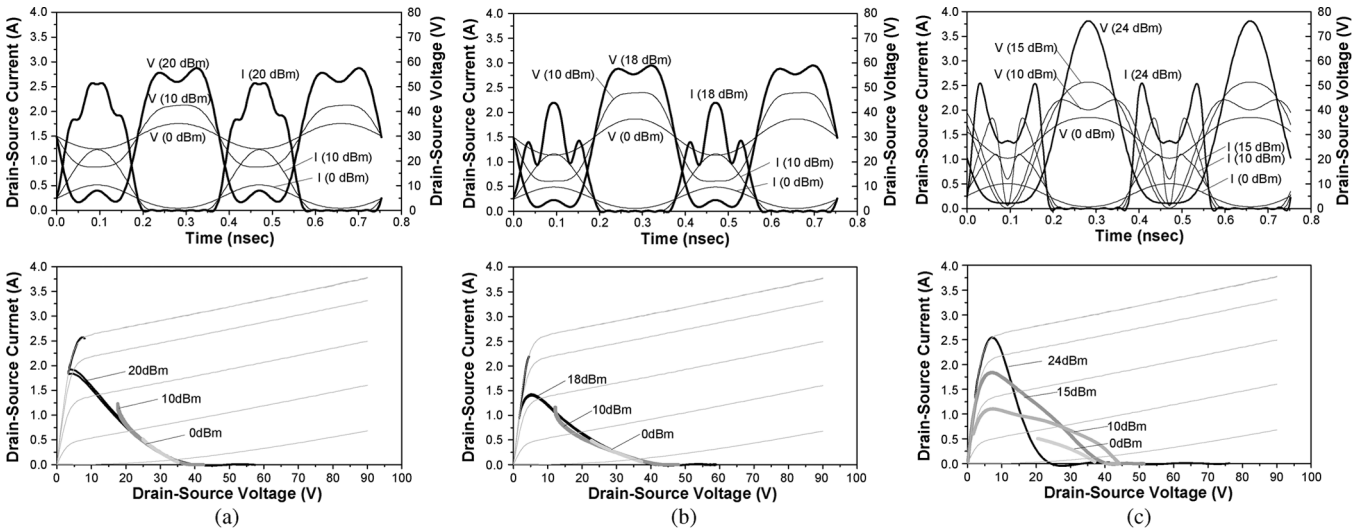

Fig. 11. Simulated voltage and current waveforms and load-lines of: (a) class-F, (b) class-F with the $R_{\mathrm{opt,F^{-1}}}$, and (c) class-F^{-1} amplifiers.

are out-of-phase even at a low input power level, the proper voltage shape is carried out earlier for the class-F amplifier, and at the input power of 10 dBm, the two class-F amplifiers have the proper voltage waveforms. However, the second harmonic current is in-phase at the low input power and the voltage waveform for the class-F^{-1} amplifier is in the reversed half-sinusoidal waveform. Even though the fundamental load impedance of the class-F^{-1} amplifier is the same as the class-F amplifier with $R_{\mathrm{opt,F^{-1}}}$, the fundamental voltage component at this power level is smaller. This improper operation also deteriorates the current waveform, as shown in Fig. 11(c), reducing the fundamental current. The proper phase relationship of the currents is obtained above 20 dBm, and the half-sinusoidal voltage waveform is achieved, increasing the fundamental voltage. In addition, the properly shaped voltage waveform also generates the properly shaped current waveform, as shown in Fig. 11(c), thereby continuously enhancing the fundamental current and voltage as the power level increases. Due to the harmonic load, the class-F^{-1} amplifier operates as a saturated amplifier at the high power region, following the bifurcated current waveform, but the bifurcation is limited due to the second harmonic voltage.

However, the current waveform of the class-F amplifier should be different from the bifurcated waveform. Due to the shorted second harmonic load, the second harmonic voltage cannot be supported, but only the third harmonic voltage can. Therefore, the device operates as a switch in the saturated region, as shown in Fig. 11(a) and (b). The fundamental load impedance of the class-F amplifier with the $R_{\mathrm{opt,F^{-1}}}$ is larger than that of the class-F amplifier and its maximum fundamental current is lower, but the fundamental voltage is slightly increased due to the low knee voltage.

Fig. 12 shows the simulated performances of the amplifiers. At a high power, the fundamental currents of the class-F amplifiers are maintained, but the dc currents are increased as the input power enlarges, degrading the efficiency with constant output powers [see Fig. 12(a) and (b)]. Due to the larger fundamental load impedance of the class-F amplifier with $R_{\mathrm{opt,F^{-1}}}$, the output power is lower than that of the class-F amplifier. For the class-F^{-1} amplifier, even though the fundamental current is a little low, the fundamental voltage is increased up to $\sqrt{2}$ times the fundamental voltage of the tuned load PA. Thus, the output power of the class-F^{-1} amplifier at the high power region is larger than the others. However, the improper phase relation of the currents at the low power region reduces the output power, degrading the gain and efficiency. The class-F amplifier with the $R_{\mathrm{opt,F^{-1}}}$ and class-F^{-1} amplifiers have the same knee voltage effect. Thus, the maximum efficiencies of the amplifiers is nearly the same. At a high drive level, the fundamental current of the class-F^{-1} amplifier increases together with the dc current. Therefore, the output power increases with near constant efficiency. Overall, the class-F^{-1} PA can deliver the best output power and efficiency performances at the cost of the larger voltage swing.

B. Class-F Amplifier With Nonlinear Capacitor

The input and output nonlinear capacitors, shown in Fig. 6(c) and (d), change according to the input power level. C_{IN}, including the nonlinear gate–source capacitor and gate–drain capacitor transferred by the Miller effect, increases as the gate–source voltage increases. Although this capacitor changes also with the drain–source voltage, we assume the gate–source voltage dependent change only for simplicity. C_{OUT}, consisted of the nonlinear drain–source capacitor and Miller transferred gate–drain capacitor, decreases as the drain–source voltage increases. These nonlinear capacitors generate the harmonic voltage components at the input and output of the transistor. Those harmonic components are pretty large and change the operational behaviors of the amplifiers.

Nonlinear C_{IN} generates the harmonics with some phase. Thus, the harmonic load should be adjusted for the phase and is no longer resistive. Nonlinear C_{OUT} also generates a large second harmonic with smaller high-order harmonics. The capacitor also contributes to the current shaping because the nonlinear capacitance is the voltage-dependent output load.

1) Effects of the Nonlinear Input Capacitor: To explore the influence of the nonlinear input capacitor on the Class-F amplifier, the third harmonic load–pull simulation is carried

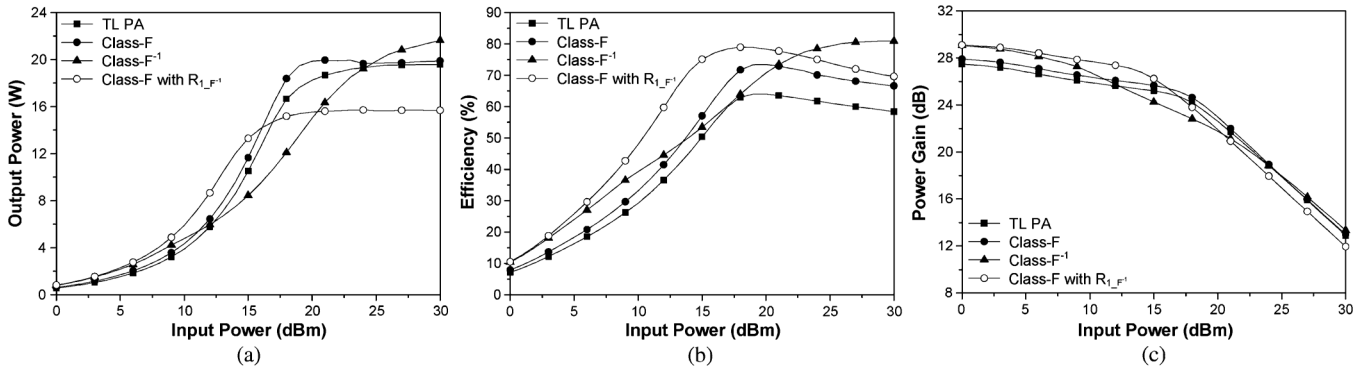

Fig. 12. Simulated: (a) output power, (b) efficiency, and (c) power gain performances of class-F, class-F with $R_{\mathrm{opt,F^{-1}}}$, class-F^{-1}, and tuned load PA according to the input power level.

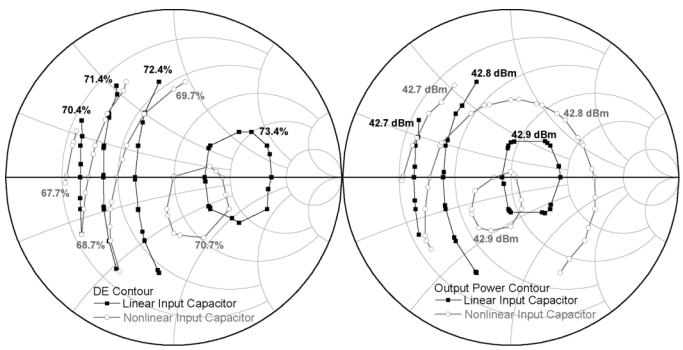

Fig. 13. Third harmonic load–pull simulation results: efficiency and output power contours of class-F PA with the linear and nonlinear input capacitors.

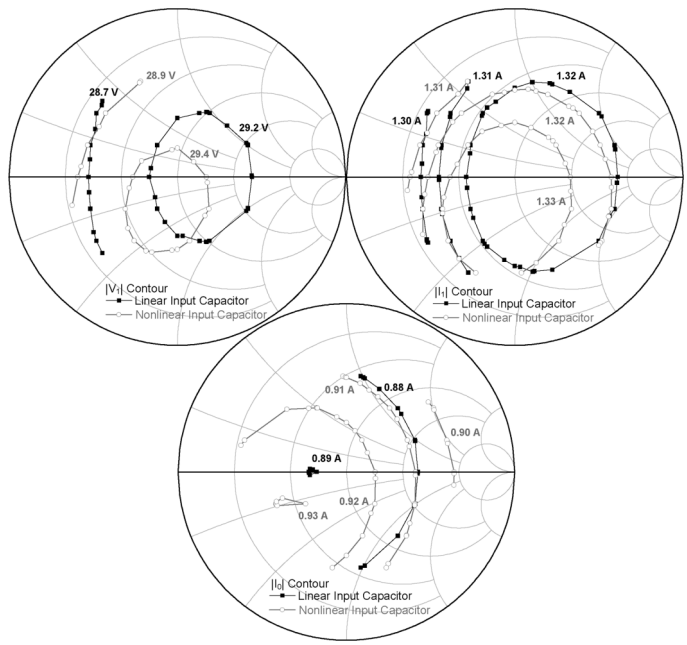

Fig. 14. Third harmonic load–pull simulation results: $|V_1|$, $|I_1|$, and $|I_0|$ contours of class-F PA with the linear and nonlinear input capacitors.

out, for simplicity, without the linear output capacitor. As the input power increases, the capacitance of the nonlinear capacitor also enlarges, degrading the gain performance. Thus, for the load–pull simulation, the input powers of the PAs with the linear and nonlinear capacitors are set to 20 and 24 dBm, respectively. The fundamental load impedances for both PAs are adjusted to provide the maximum efficiency. All harmonic impedances at the source are shorted, which is nearly the optimum condition.

Fig. 13 shows the efficiency and output power contours and Fig. 14 depicts $|V_1|$, $|I_1|$, and $|I_0|$ contours of the class-F amplifier with the linear and nonlinear input capacitors, respectively. $|V_1|$, $|I_1|$, and $|I_0|$ represent the magnitudes of the fundamental voltage, fundamental current, and dc current, respectively. The nonlinear input capacitor changes the phase relation between the fundamental and third harmonic currents, and the optimum third harmonic impedance for the high efficiency and output power is not purely resistive. Since the nonlinear input capacitor generates the in-phased second harmonic, the voltage across the capacitor becomes the reversed half-sinusoidal shape. Thus, the effective conduction angle is increased, decreasing the efficiency. As the input power increases, the input capacitance also increases, reducing the gain. In addition, due to the enlarged effective conduction angle caused by the nonlinear capacitor, the maximum $|V_1|$ and $|I_1|$ of the amplifier with the nonlinear capacitor are increased. Therefore, the maximum output power is slightly increased by 0.06 dBm, to 42.942 dBm. However, the maximum $|I_0|$ is quite larger and the maximum efficiency is somewhat lowered.

2) Effects of the Nonlinear Output Capacitor: To explore the influence of the nonlinear C_{OUT} on the class-F amplifier, the third harmonic load–pull simulation is carried out when C_{IN} is nonlinear. The fundamental load impedances for the amplifiers with the linear and nonlinear output capacitors are adjusted to maximize the output power at the input power of 24 dBm. The fundamental source impedances of the amplifiers are conjugately matched to deliver the maximum power to the input of the transistor. Fig. 15 shows the efficiency and output power contours of the class-F amplifier with linear and nonlinear output capacitors and Fig. 16 illustrates $|V_1|$, $|I_1|$, and $|I_1|/|I_0|$ contours of the amplifier. Even though the maximum $|V_1|$ and $|I_1|$ of the PA with the nonlinear C_{OUT} are similar to the PA with the linear capacitor, the PA with the nonlinear capacitor has larger $|V_1|$ and $|I_1|$ over a wider impedance level. Apparently, such characteristics are caused by the harmonic generation of the nonlinear capacitor. In this region, the ratio of $|I_1|$ and $|I_0|$ of the PA with the nonlinear output capacitor is slightly larger than the PA with linear output capacitor, resulting in higher efficiency over a wider impedance level. Fig. 17 shows the simu-

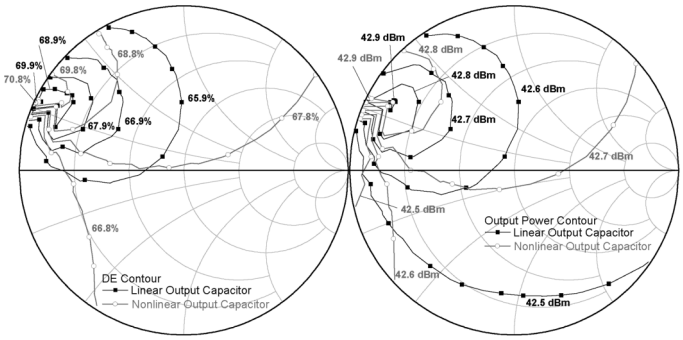

Fig. 15. Third harmonic load–pull simulation results: efficiency and output power contours of class-F PA with the linear and nonlinear output capacitors.

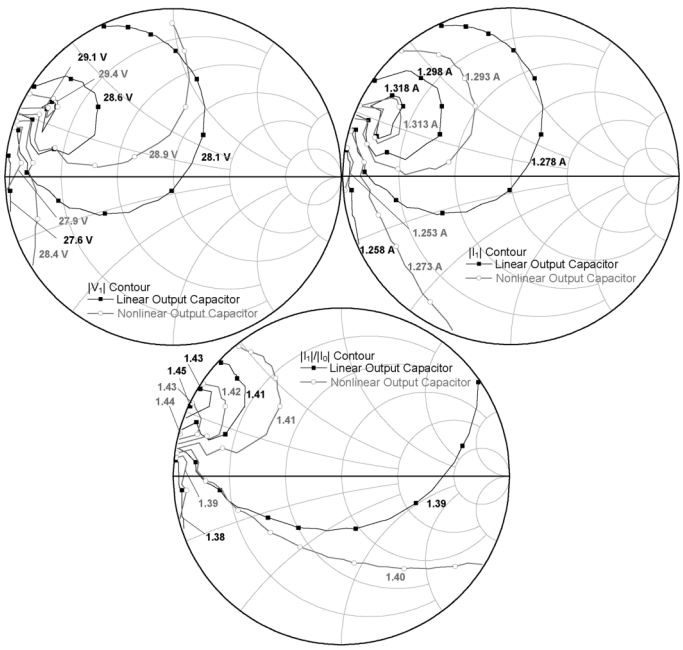

Fig. 16. Third harmonic load–pull simulation results: $|V_1|$, $|I_1|$, and $|I_1|/|I_0|$ contours of class-F PA with the linear and nonlinear output capacitors.

lated fundamental voltage, fundamental current, output power, and efficiency characteristics of the class-F amplifier with the linear and nonlinear C_{OUT}. Since the nonlinear output capacitor generates a large second harmonic with a small third harmonic, both PAs provide nearly the same performance. Fig. 18 represents the voltage and current waveforms when the amplifiers deliver the maximum efficiency.

C. Class-F^{-1} Amplifier with Nonlinear Capacitor

1) Effects of the Nonlinear Input Capacitor: Similarly to the Class-F amplifier, the nonlinear input capacitor increases the effective conduction angle. Therefore, the dc and fundamental currents and fundamental voltage are enlarged. Since the efficiency is maintained for the conduction angle, as shown in numerical analysis results for the Class-F^{-1} PA in Section II-A, the efficiencies of the two PAs are nearly the same. The results are summarized in Table I.

2) Effects of the Nonlinear Output Capacitor: To explore the influence of the nonlinear output capacitor on the class-F^{-1} amplifier, the second harmonic load–pull simulation is carried out for the model with the nonlinear input capacitor. Fundamental load impedances for the PAs with the linear and nonlinear output

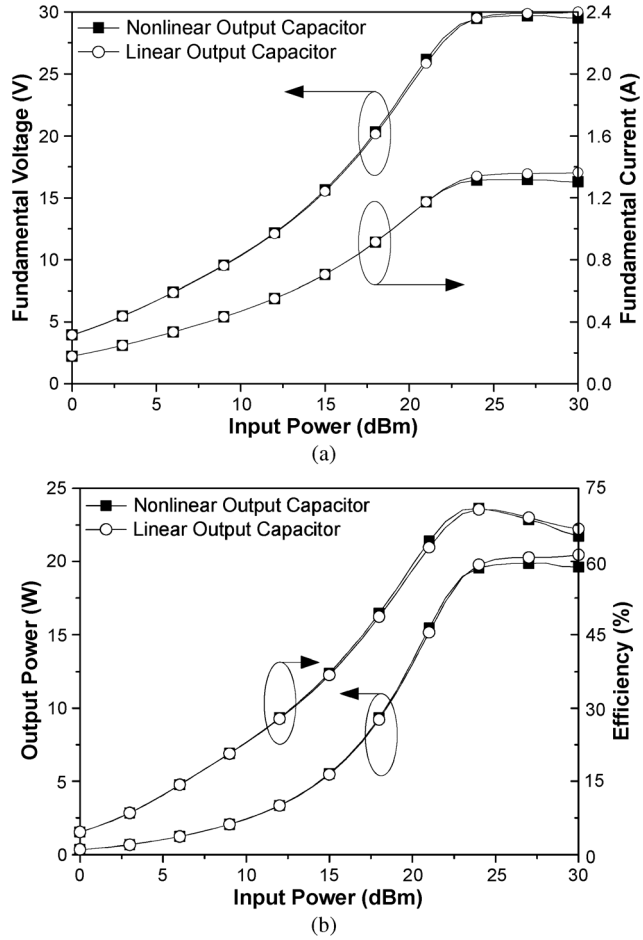

Fig. 17. Simulated: (a) fundamental voltage and current and (b) output power and efficiency characteristics of class-F PAs with the linear and nonlinear output capacitor according to the input power.

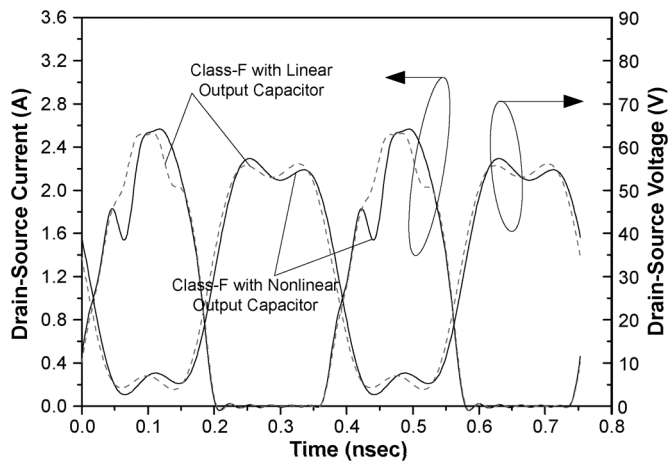

Fig. 18. Simulated voltage and current waveforms of class-F PA with the linear and nonlinear output capacitors at the input power of 25 dBm.

capacitors are adjusted to maximize the output power. In order to deliver the maximum input power to the transistor at the maximum power level, the fundamental source impedances of the both PAs are conjugately matched. The simulations are conducted at the input power of 27.7 dBm. Fig. 19 shows $|V_1|$, $|I_1|$, and $|I_1|/|I_0|$ contours of the class-F^{-1} amplifier with the linear and nonlinear output capacitors. Similarly to the class-F amplifier, the class-F^{-1} amplifier with the nonlinear capacitor has

TABLE I
FUNDAMENTAL AND DC COMPONENTS OF THE CURRENT AND VOLTAGE OF THE CLASS-F AND CLASS-F^{-1} AMPLIFIERS WITH LINEAR AND NONLINEAR INPUT CAPACITORS

	$\lvert V_1\rvert$ (V)	$\lvert V_{\rm DC}\rvert$ (V)	$\lvert V_1/V_{\rm DC}\rvert$	$\lvert I_1\rvert$ (A)	$\lvert I_{\rm DC}\rvert$ (A)	$\lvert I_1/I_{\rm DC}\rvert$	Efficiency (%)	Output Power (W)
Class-F with Linear Input Capacitor	29.33	30	0.978	1.33	0.89	1.494	73.1	19.5
Class-F with Nonlinear Input Capacitor	29.53	30	0.984	1.34	0.93	1.441	70.9	19.8
Class-F^{-1} with Linear Input Capacitor	37.13	30	1.238	1.08	0.82	1.317	81.5	20.1
Class-F^{-1} with Nonlinear Input Capacitor	37.84	30	1.261	1.10	0.85	1.294	81.6	20.8

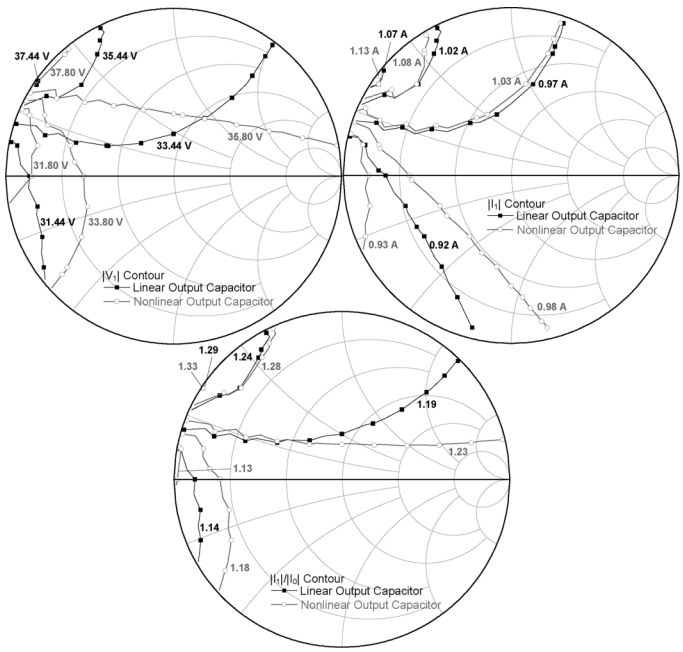

Fig. 19. Second harmonic load–pull simulation results: $|V_1|$, $|I_1|$, and $|I_1|/|I_0|$ contours of class-F^{-1} PA with linear and nonlinear output capacitors.

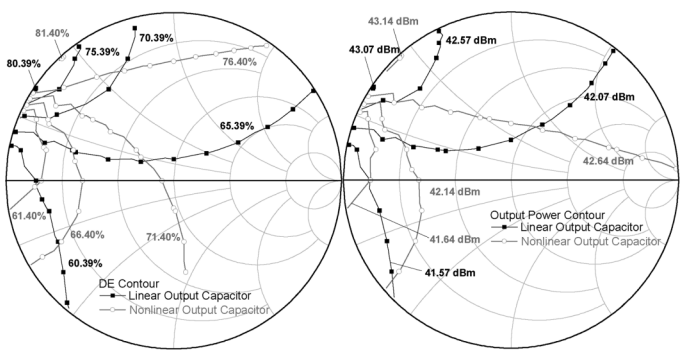

Fig. 20. Second harmonic load–pull simulation results: efficiency and output power contours of class-F^{-1} PA with linear and nonlinear output capacitors (the second harmonic load–pull).

larger $|V_1|$ and $|I_1|$ over a wider region on the Smith chart. In addition, the ratio of $|I_1|$ to $|I_0|$ of the amplifier is larger than that of the class-F^{-1} amplifier with the linear capacitor, resulting in larger efficiency and output power across the wider impedance level, as shown in Fig. 20.

Fig. 21(a) shows the simulated fundamental voltage and current characteristics of the class-F^{-1} amplifier with the linear and nonlinear $C_{\rm OUT}$. It shows an interesting result; the amplifier with the nonlinear output capacitor generates higher

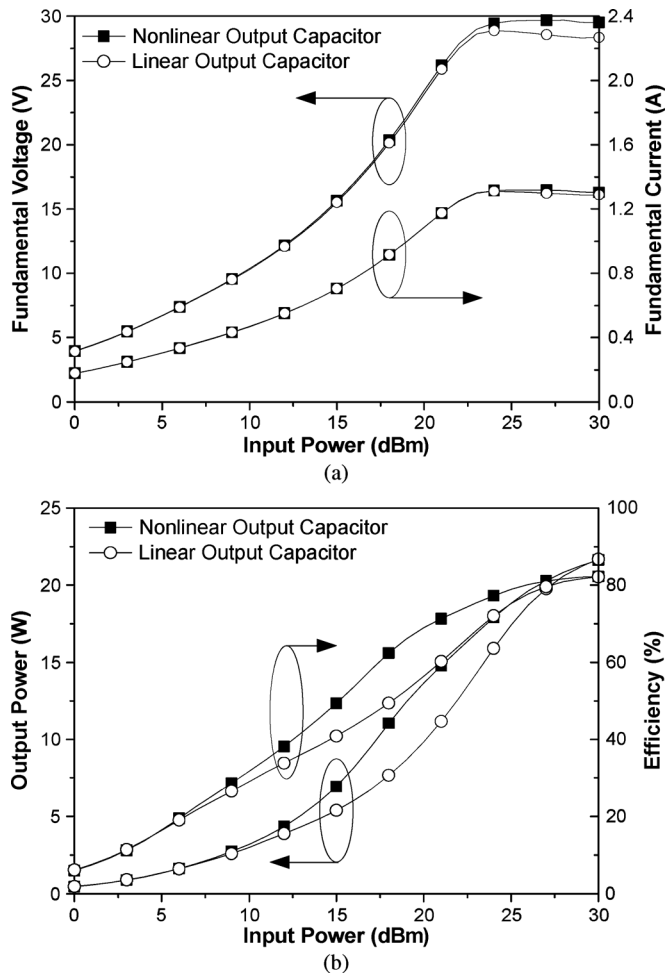

Fig. 21. Simulated: (a) fundamental voltage and current and (b) output power and efficiency characteristics of class-F^{-1} PA with linear and nonlinear output capacitors according to the input power.

fundamental voltage even though the PA is not driven into the highly saturated region. In this low power region, the phase relation between the fundamental and second harmonic currents are in phase. Thus, if we assume that the voltage is generated by the current and load impedance, the proper half-sinusoidal voltage waveform can not be achieved. However, due to the harmonic generation of the nonlinear output capacitor, the PA with the nonlinear capacitor can provide the proper half-sinusoidal voltage shape, increasing the output power and efficiency. The current shaping is achieved through the saturated operation, as shown in Fig. 11(c), with a large load impedance, larger than $\sqrt{2}\cdot R_{\rm opt,TL}$ contrary to the lower load $0.785\cdot R_{\rm opt,TL}$ of

the conventional class-F^{-1} amplifier. The voltage shaping is mainly accomplished by the nonlinear output capacitor and the harmonic load assists to obtain the optimum efficiency. These behaviors are quite different from the conventional class-F^{-1} PA. This amplifier is the optimized version at the saturated operation, and we have already introduced these kinds of PAd as a saturated amplifier [3], [19]–[21]. The proper voltage waveform shaping assisted by the output capacitor generates the proper current waveform also, increasing the fundamental current. Thus, the amplifier delivers higher efficiency and output power than the PA with the linear capacitor from the medium to high power levels, as shown in Fig. 21(b). At the maximum power region, the saturated operation itself can generate enough second harmonic current and the two PAs deliver the same performance. Fig. 22 shows the simulated voltage and current waveforms of the class-F^{-1} amplifier with the linear and nonlinear output capacitors at the input power of 10, 20, and 28 dBm. For the PA with the linear capacitor, due to the improper phase relationship of the currents, the proper voltage waveform is not generated at the low power, leading to the deeply saturated current waveform. However, with the nonlinear output capacitor, the half-sinusoidal voltage waveform is maintained even at the low power.

As shown in Fig. 23, the fundamental voltage component of the saturated amplifier is larger than that of the class-F amplifier over the power levels, although the current is somewhat limited. Therefore, the saturated PA outperforms the class-F PA. The gain is higher at a lower power, but is compressed faster.

D. Summary

In this section, the characteristics of the class-F and class-F^{-1} amplifiers with the linear and nonlinear capacitors are summarized. The harmonics generated by the nonlinear capacitor significantly change the operational behaviors of the amplifiers. The nonlinear input capacitor enlarges the effective conduction angle, increasing the output power. The efficiency is maintained for the class-F^{-1} amplifiers, but is decreased for the class-F amplifier, as summarized in Table I. The nonlinear output capacitor generates a large second harmonic voltage with smaller high-order terms. Thus, the class-F amplifiers with the linear and nonlinear output capacitors provide the similar performance, as shown in Fig. 17. However, the tolerance for the harmonic load is increased due to the third harmonic voltage generated by the nonlinear capacitor, and the amplifier with the nonlinear capacitor has a little higher output power and efficiency across the broad third harmonic load impedance, as shown in Fig. 15. Similar to the class-F amplifier, the class-F^{-1} amplifier with the nonlinear capacitor also has a large tolerance for the second harmonic load, as shown in Fig. 20. Although the class-F^{-1} amplifier with the linear output capacitor cannot generate the proper half-sinusoidal voltage waveform below the deeply saturated input power level, as shown in Fig. 22, the amplifier with the nonlinear output capacitor can because the capacitor generates the proper second harmonic voltage, forming the half-sinusoidal voltage waveform even at the low input power level. Thus, the amplifier has larger fundamental voltage and current at the low power level, increasing the output power and efficiency, as shown in Fig. 21. Moreover, the fundamental load

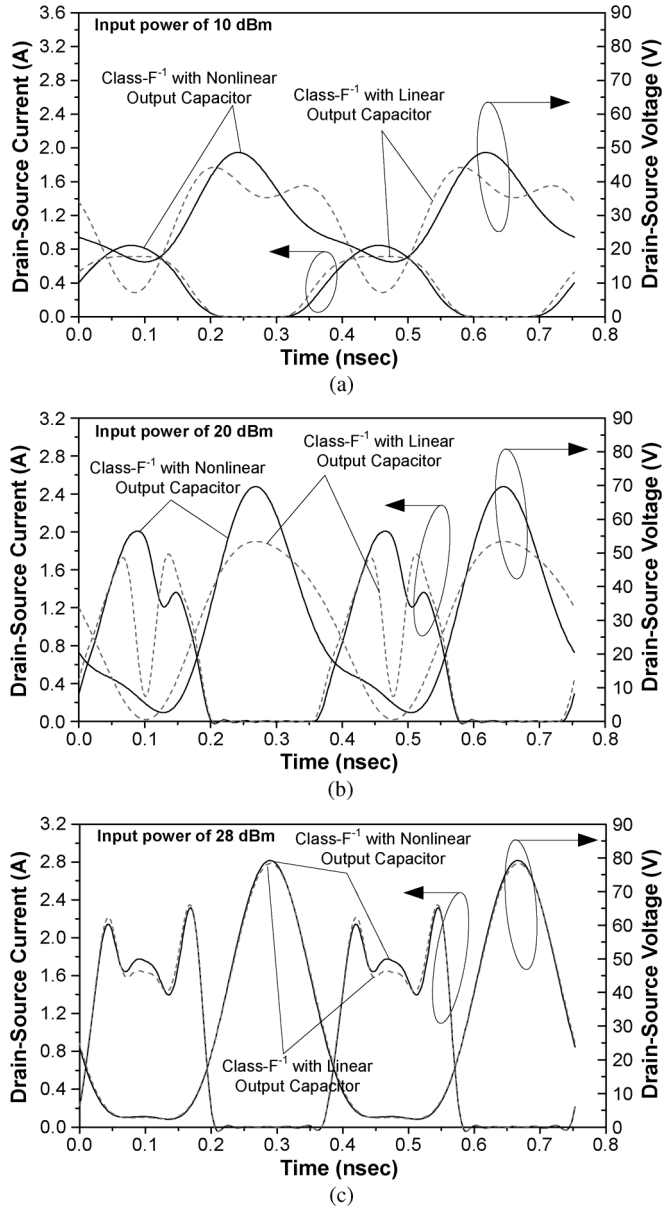

Fig. 22. Simulated voltage and current waveforms of class-F^{-1} PA with linear and nonlinear output capacitors at the input power of: (a) 10 dBm, (b) 20 dBm, and (c) 28 dBm.

should be a lot larger than the tuned load amplifier contrary to the lower load in the conventional wisdom. The deeply saturated operation provides the quasi-rectangle current with a reduced bifurcated current. Since the amplifier takes advantage of the nonlinear output capacitor to shape the voltage waveform, it has large tolerance for the harmonic load. As we described in [3], the second harmonic load at the current source is opened and the third harmonic is shorted by the large output capacitance. The higher order terms have a minor effect on the performance. The operation mechanism of the class-F^{-1} amplifier, we have discovered thus far, is quite different from the conventional class-F^{-1} amplifier. This mode of operation is the optimized power operation in the saturated mode, and we call it the saturated amplifier. There are several PAs optimized using the load–pull data in [22] and [23], and those amplifier are the saturated amplifiers, supporting our claim.

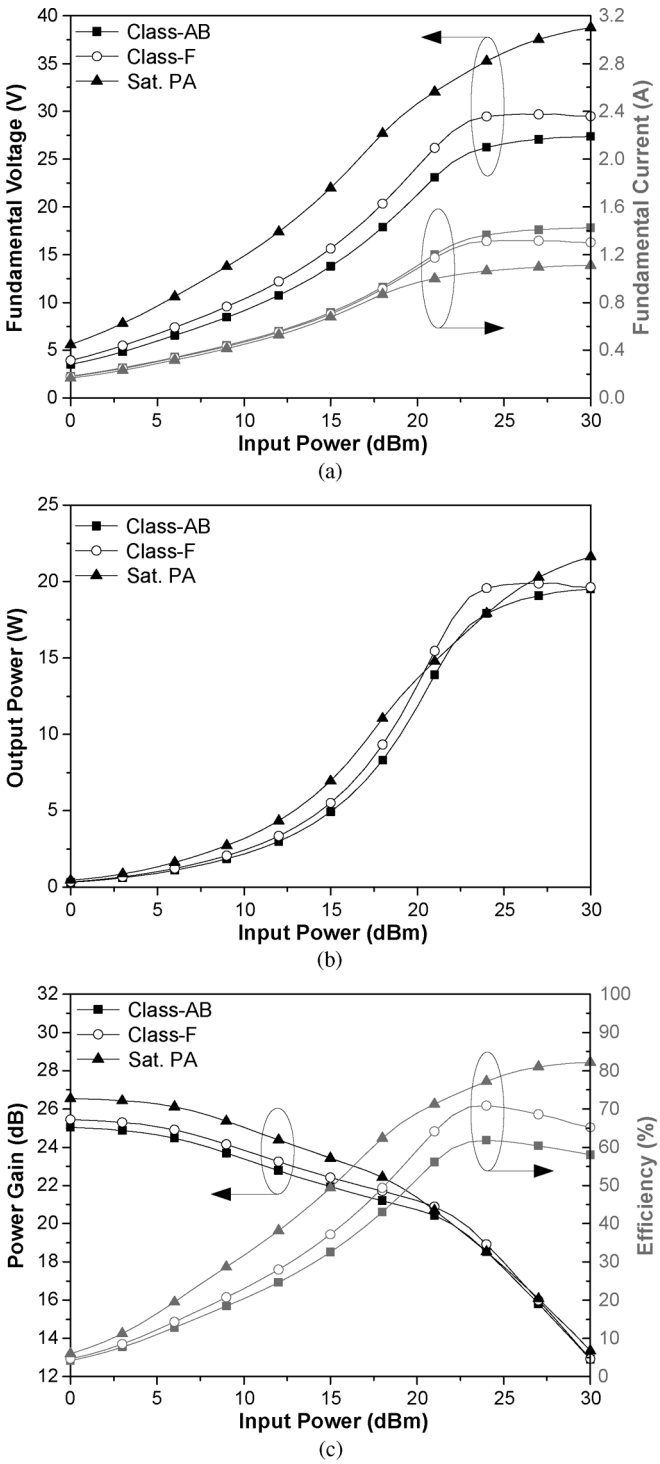

Fig. 23. Simulated performance comparisons of tuned load PA, class-F PA, and saturated PAs with the input and output nonlinear capacitors. (a) Fundamental voltage and current. (b) Output power. (c) Power gain and efficiency.

Figs. 12 and 21 show the simulated continuous wave (CW) performance of the amplifiers with the linear and nonlinear capacitors, respectively. Since the nonlinear output capacitor generates the proper second harmonic voltage component, the saturated amplifier can have the half-sinusoidal voltage waveform for all input power levels, and the fundamental voltage is larger than those of others. Moreover, the fundamental voltage increases with input power drive although the current level is saturated. Due to the larger fundamental load impedance of the saturated amplifier, it has lower maximum current. Thus, compared with the other amplifiers, the saturated amplifier has the heavily compressed gain characteristic, but delivers the higher output power and efficiency, as shown in Fig. 23. These simulation results show that the saturated amplifier is the better suited architecture for the high-efficiency PA at a high frequency.

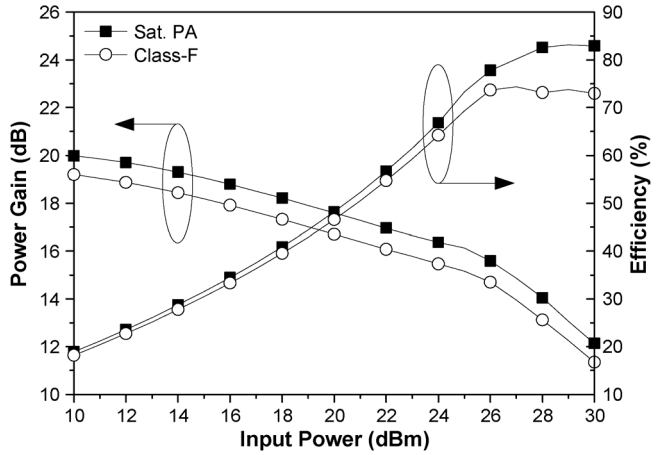

Fig. 24. Simulated efficiencies and power gains of the class-F and saturated amplifiers using a real device.

IV. Implementation and Experimental Results

In Section III, the class-F and class-F^{-1} amplifiers with the nonlinear capacitor are investigated. To validate the voltage waveform shaping by the nonlinear output capacitor and the highly efficient operation of the saturated amplifier, we designed and implemented the amplifier at 2.655 GHz using the Cree GaN HEMT CGH40010 packaged device containing a CGH60015 bare die. Since the commercial device model includes the package effects such as the bonding wires, package leads, and parasitics, the simulation is carried out using the bare-chip model to explore the inherent operation of the saturated amplifier. In addition, the saturated amplifier is compared with the class-F amplifier using the bare-chip model. For the implementation, the packaged device containing the bare chip is employed for simulation and to build the amplifier.

Fig. 24 shows the simulated efficiencies and power gains of the class-F and saturated amplifiers using the bare-chip model. As expected, the saturated amplifier delivers the improved gain and efficiency characteristic compared to the class-F amplifier. However, the gain compression is not that fast. The efficiency curves for the two PAs are also similar to the previous simulation result in Section III. Fig. 25 shows the second harmonic load–pull contours and time-domain voltage and current waveforms of the saturated amplifier using the bare-chip model. During the simulation, the fundamental and third harmonic loads are set to $11.95 + j20\,\Omega$ and $0.7 - j31.7\,\Omega$, respectively. Due to the harmonic generation of the nonlinear output capacitor, the high efficiency is maintained across the wide second harmonic impedance region. Moreover, even if the input power is low, the half sinusoidal voltage waveform is generated, proving the harmonic generation by the nonlinear output capacitor.

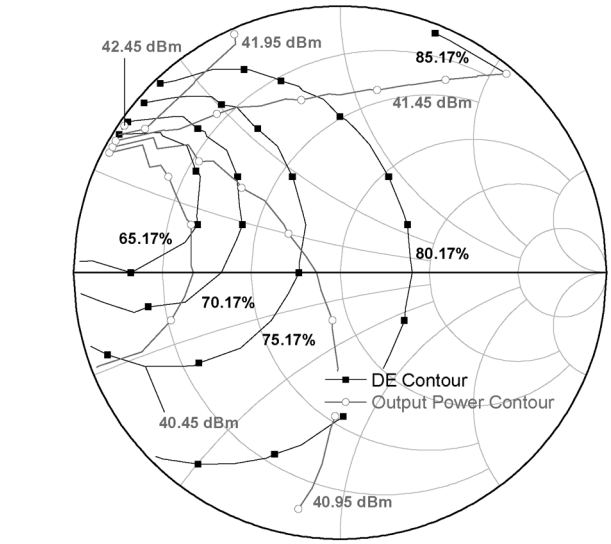

(a)

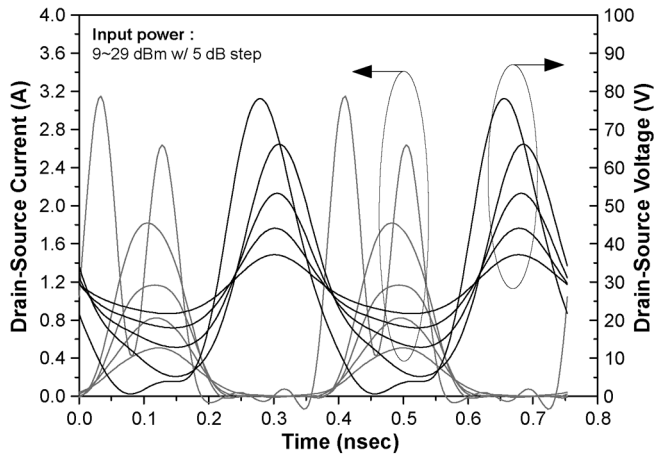

(b)

Fig. 25. Real device simulation results. (a) Second harmonic load–pull contours. (b) Time-domain voltage and current waveforms of the saturated PA.

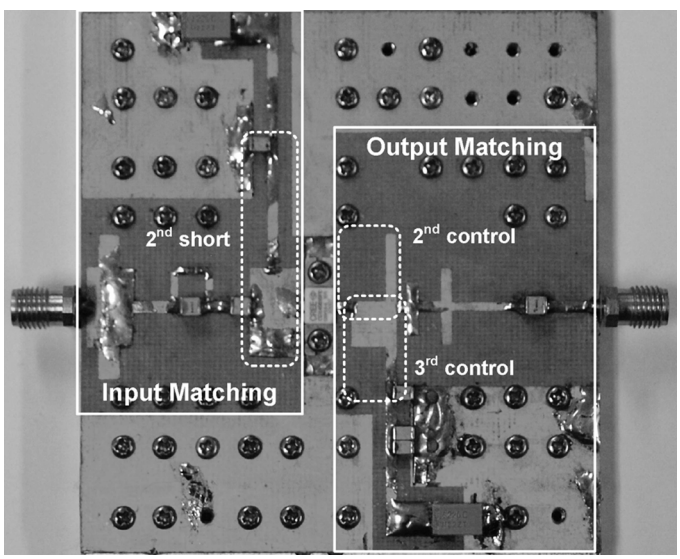

Fig. 26. Photograph of implemented saturated amplifier.

Fig. 26 shows a photograph of the implemented saturated amplifier. The amplifier is built on an RF-35 substrate with

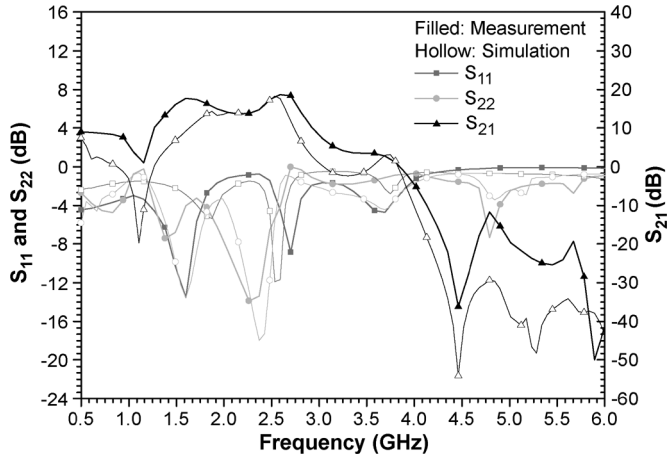

Fig. 27. Simulated and measured S-paramenters.

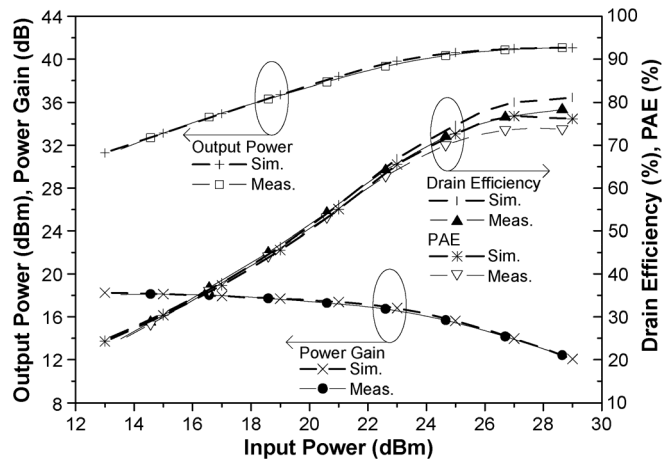

Fig. 28. Simulated and measured output power, drain efficiency, PAE, and power gain.

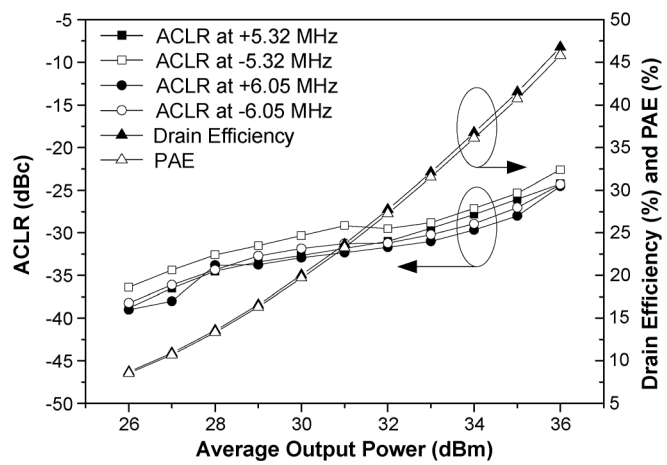

Fig. 29. Measured ACLR, drain efficiency, and PAE when the implemented PA is excited by m-WiMAX signal.

$\varepsilon_r = 3.5$ and thickness of 30 mil. In the experiment, the amplifier is biased at -2.1 V ($I_{\mathrm{DSQ}} = 210$ mA, conduction angle of about 190°) at a supplied drain voltage of 28 V. The amplifier provides a maximum power-added efficiency (PAE) of 73.5% at a saturated output power of 41 dBm. Moreover, the well-matched small-signal characteristics between the measurement and simulation are shown in Fig. 27. The simulated and measured output power, efficiency, and gain characteristics for

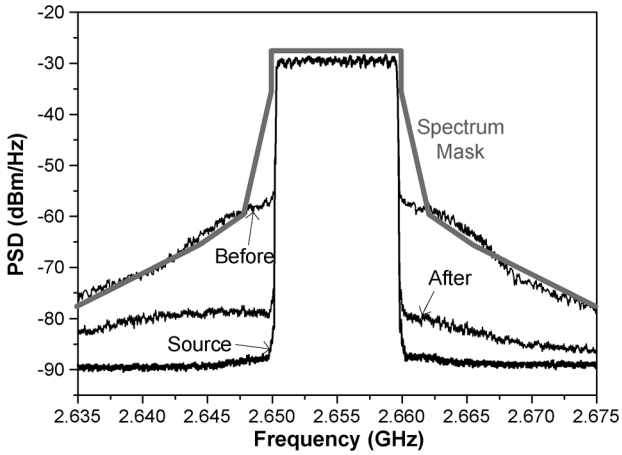

Fig. 30. Measured spectras at an average output power of 33.5 dBm before and after linearization.

TABLE II
LINEARIZATION PERFORMANCE AT AN AVERAGE OUTPUT POWER OF 33.5 dBm FOR m-WiMAX SIGNAL

	ACLR		RCE	PAE
	5.32 MHz (dBc)	6.05 MHz (dBc)	(dB)	(%)
Before	–27.7	–29.2	–24.2	33.6
After	–49.3	–50.1	–35.1	34.0

a CW signal are also well matched, as shown in Fig. 28. Fig. 29 depicts the measured adjacent channel leakage ratio (ACLR) and efficiencies for mobile world wide interoperability for microwave access signal with 7.7-dB peak-to-average power ratio and 10-MHz signal bandwidth. The amplifier delivers a PAE of 33.6% at an average output power of 33.5 dBm. To validate potential of the implemented amplifier as a main block of a linear femto-cell application, the linearization of the amplifier is conducted using a digital feedback predistortion technique [24]. Fig. 30 illustrates the measured output spectra before and after the linearization. The ACLRs at the offset frequencies of 5.32 and 6.05 MHz are -49.3 and -50.1 dBc, respectively, which are improvements of 21.6 and 20.9 dB, respectively, at an average output power of 33.5 dBm. The linearization results are summarized in Table II.

V. CONCLUSIONS

The operational behaviors of the class-F and class-F^{-1} amplifiers have been analyzed. The analysis are conducted through the numerical description for the current sources and simulations using the simplified transistor models with the linear and nonlinear capacitors. In the numerical description, the output power, efficiency, and gain characteristics of the amplifiers are compared according to the conduction angle. In addition, the optimum load impedances and input overdrive ratios are derived. The numerical analysis is then validated using the simplified real device model. With the nonlinear capacitor, the amplifiers are investigated according to the power level. Since the capacitor generates harmonics, a large second harmonic voltage with smaller high-order terms, the operational behaviors are changed in comparison with the amplifiers with the linear capacitor. The operation of the class-F^{-1} amplifier with the nonlinear output capacitor is especially quite different from that of the classical class-F^{-1} PA, in which the voltage shaping is carried out by the large second harmonic voltage. Thus, the class-F^{-1} amplifier with the nonlinear capacitor has the half-sinusoidal voltage waveform even at the low power level. Compared to the class-F amplifier, the class-F^{-1} amplifier delivers superior performance due to its larger fundamental voltage. The simulation results lead to the conclusion that the nonlinear output capacitor is important element for the class-F^{-1} amplifier for the voltage shaping. The class-F^{-1} amplifier we have defined is quite different from the classical class-F^{-1} amplifier, which is not clearly defined for practical design, because the voltage-shaping mechanisms and the fundamental load are not the same. We have called it the saturated amplifier since this amplifier is the optimized structure for high efficiency. To validate the voltage waveform shaping by the nonlinear output capacitor and the highly efficient operation of the saturated amplifier, we designed and implemented the amplifier at 2.655 GHz. It provides a maximum PAE of 73.5% at a saturated output power of 41 dBm.

ACKNOWLEDGMENT

The authors would like to thank Cree Inc., Durham, NC, for providing the GaN HEMT transistors and models used in this study.

REFERENCES

[1] S. C. Cripps, *RF Power Amplifiers for Wireless Communications*, 2nd ed. Norwood, MA: Artech House, 2006.
[2] J. Choi, D. Kang, D. Kim, J. Park, B. Jin, and B. Kim, "Power amplifiers and transimitters for next generation mobile handset," *J. Semicond. Technol. Sci.*, vol. 9, no. 4, pp. 249–256, Dec. 2009.
[3] S. Jee, J. Moon, J. Kim, J. Son, and B. Kim, "Switching behavior of class-E power amplifier and its operation above maximum frequency," *IEEE Trans. Microw. Theory Tech.*, vol. 60, no. 1, pp. 89–98, Jan. 2012.
[4] T. B. Mader and Z. B. Popović, "The transmission-line high-efficiency class-E amplifier," *IEEE Microw. Guided Wave Lett.*, vol. 5, no. 9, pp. 290–292, Sep. 1995.
[5] E. Cipriani, P. Colantonio, F. Giannini, and R. Giofrè, "Optimization of class E power amplifier design above theoretical maximum frequency," in *Proc. 38th Eur. Microw. Conf.*, Oct. 2008, pp. 1541–1544.
[6] E. Cipriani, P. Colantonio, F. Giannini, and R. Giofrè, "Theory and experimental validation of a class E PA above theoretical maximum frequency," *Int. J. Microw. Wireless Technol.*, vol. 1, no. 4, pp. 293–299, Jun. 2009.
[7] A. L. Clarke, M. Akmal, J. Lees, P. J. Tasker, and J. Benedikt, "Investigation and analysis into device optimization for attaining efficiencies in-excess of 90% when accounting for higher harmonics," in *IEEE MTT-S Int. Microw. Symp. Dig.*, Jun. 2010, pp. 1114–1117.
[8] A. Sheikh, C. Roff, J. Benedikt, P. J. Tasker, B. Noori, J. Wood, and P. H. Aaen, "Peak class F and inverse class F drain efficiencies using Si LDMOS in a limited bandwidth design," *IEEE Microw. Wireless Compon. Lett.*, vol. 19, no. 7, pp. 473–475, Jul. 2009.
[9] C. J. Wei, P. DiCarlo, Y. A. Tkachenko, R. McMorrow, and D. Bartle, "Analysis and experimental waveform study on inverse class class-F mode of microwave power FETs," in *IEEE MTT-S Int. Microw. Symp. Dig.*, Jun. 2000, pp. 525–528.
[10] A. Inoue, T. Heima, A. Ohta, R. Hattoru, and Y. Mitsui, "Analysis of class-F and inverse class-F amplifiers," in *IEEE MTT-S Int. Microw. Symp. Dig.*, Jun. 2000, pp. 775–778.
[11] A. Inoue, A. Ohta, S. Goto, T. Ishikawa, and Y. Matsuda, "The efficiency of class-F and inverse class-F amplifiers," in *IEEE MTT-S Int. Microw. Symp. Dig.*, Jun. 2004, pp. 1947–1950.

[12] S. Goto, T. Kunii, A. Ohta, A. Inoue, Y. Hosokawa, R. Hattori, and Y. Mitsui, "Effect of bias condition and input harmonic termination on high efficiency inverse class-F amplifiers," in *Proc. 31th Eur. Microw. Conf.*, Sep. 2010, pp. 1–4.
[13] Y. Y. Woo, Y. Yang, and B. Kim, "Analysis and experiments for high-efficiency class-F and inverse class-F power amplifiers," *IEEE Trans. Microw. Theory Tech.*, vol. 54, no. 5, pp. 1969–1974, May 2006.
[14] E. Cipriani, P. Colantonio, F. Giannini, and R. Giofrè, "Class F^{-1} PA: Theoretical aspects," in *Integr. Nonlinear Microw. Millimeter-Wave Circuits Workshop*, Apr. 2010, pp. 29–32.
[15] E. Cipriani, P. Colantonio, F. Giannini, and R. Giofrè, "Theoretical and experimental comparison of class F versus class F^{-1} PAs," in *Proc. 40th Eur. Microw. Conf.*, Sep. 2010, pp. 428–431.
[16] J. H. Kim, G. D. Jo, J. H. Oh, Y. H. Kim, K. C. Lee, and J. H. Jung, "Modeling and design methodology of high-efficiency class-F and class-F^{-1} power amplifiers," *IEEE Trans. Microw. Theory Tech.*, vol. 59, no. 1, pp. 153–165, Jan. 2011.
[17] P. Colantonio, F. Giannini, G. Leuzzi, and E. Limiti, "On the class-F power amplifier design," *Int. J. RF Microw. Comput.-Aided Eng.*, vol. 9, no. 2, pp. 129–149, Feb. 1999.
[18] P. Colantonio, F. Giannini, G. Leuzzi, and E. Limiti, "High efficiency low-voltage power amplifier design by second-harmonic manipulation," *Int. J. RF Microw. Comput.-Aided Eng.*, vol. 10, no. 1, pp. 19–32, Jan. 2000.
[19] J. Moon, J. Kim, and B. Kim, "Investigation of a class-J power amplifier with a nonlinear $C_{\rm out}$ for optimized operation," *IEEE Trans. Microw. Theory Tech.*, vol. 58, no. 11, pp. 2800–2811, Nov. 2010.
[20] J. Kim, J. Kim, J. Moon, J. Son, I. Kim, S. Jee, and B. Kim, "Saturated power amplifier optimized for efficiency using self-generated harmonic current and voltage," *IEEE Trans. Microw. Theory Tech.*, vol. 59, no. 8, pp. 2049–2058, Aug. 2011.
[21] J. Moon, S. Jee, J. Kim, and B. Kim, "Investigation of a class F^{-1} power amplifier with a nonlinear $C_{\rm out}$," in *Proc. 41th Eur. Microw. Conf.*, Sep. 2011, pp. 124–127.
[22] P. Saad, H. M. Nemati, K. Andersoon, and C. Fager, "Highly efficient GaN-HEMT power amplifiers at 3.5 GHz and 5.5 GHz," in *IEEE 12th Annu. Wireless Microw. Technol. Conf.*, Apr. 2011, pp. 1–4.
[23] H. M. Nemati, C. Fager, M. Thorsell, and H. Zirath, "High-efficiency LDMOS power-amplifier design at 1 GHz using an optimized transistor model," *IEEE Trans. Microw. Theory Tech.*, vol. 57, no. 7, pp. 1647–1654, Jul. 2009.
[24] Y. Y. Woo, J. Kim, J. Yi, S. Hong, I. Kim, J. Moon, and B. Kim, "Adaptive digital feedback predistortion technique for linearizing power amplifier," *IEEE Trans. Microw. Theory Tech.*, vol. 55, no. 5, pp. 932–940, May 2007.

Junghwan Moon (S'07) received the B.S. degree in electrical and computer engineering from the University of Seoul, Seoul, Korea, in 2006, and the Ph.D. degree in electrical engineering from the Pohang University of Science and Technology (POSTECH), Pohang, Gyeongbuk, Korea, in 2012.

He is currently a Senior Engineer with the Telecommunication Systems Division, Samsung Electronics Company Ltd., Suwon, Korea. In 2011, he was a Visiting Researcher with the Giga-Hertz Centre, Microwave Electronics Laboratory, Chalmers University of Technology, Göteborg, Sweden. He has authored or coauthored over 50 papers in international journals and conference proceedings. His current research interests include linear, efficient, and wideband RF PA/transmitter design and digital predistortion (DPD) techniques.

Dr. Moon was the recipient of the Highest Efficiency Award of the 2008 Student High-Efficiency Power Amplifier Design Competition, IEEE MTT-S International Microwave Symposium (IMS), the 2011 First Place Award of the Student High-Efficiency Power Amplifier Design Competition, IEEE MTT-S IMS, and the 2012 Best Thesis Award in electrical engineering of POSTECH.

Seunghoon Jee (S'11) received the B.S. degree in electronic and electrical engineering from Kyungpook National University, Daegu, Korea, in 2009, and is currently working toward the Ph.D. degree at the Pohang University of Science and Technology (POSTECH), Pohang, Gyeongbuk, Korea.

His current research interests include highly linear and efficient RF PA design.

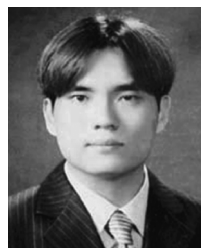

Jungjoon Kim (S'10) received the B.S. degree in electrical engineering from Han-Yang University, Ansan, Korea, in 2007, the Master degree in electrical engineering from the Pohang University of Science and Technology (POSTECH), Pohang, Gyeongbuk, Korea, in 2009, and is currently working toward the Ph.D. degree at POSTECH.

His current research interests include RF PA design and supply modulator design for highly efficient transmitter systems.

Jangheon Kim (S'07–M'09) received the B.S. degree in electronics and information engineering from Chonbuk National University, Chonju, Korea, in 2003, and the Ph.D. degree in electrical engineering from the Pohang University of Science and Technology (POSTECH), Pohang, Gyeongbuk, Korea, in 2009.

He is currently a Senior Engineer with the Systems Research and Development Team, Telecommunication Systems Division, Samsung Electronics Company Ltd., Suwon, Korea. From 2009 to 2010, he was a Post-Doctoral Fellow with the University of Waterloo, Waterloo, ON, Canada. He has authored or coauthored over 40 papers in international journals and conference proceedings. His current research interests include highly linear and efficient RF PA design, digital predistortion (DPD) techniques, and highly efficient transmitters for wireless communication systems.

Dr. Kim was the recipient of the Highest Efficiency Award of the 2008 Student High-Efficiency Power Amplifier Design Competition of IEEE MTT-S International Microwave Symposium (IMS) and the 2010 MICROWAVE AND WIRELESS COMPONENTS LETTERS Outstanding Reviewer Award.

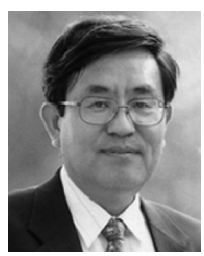

Bumman Kim (M'78–SM'97–F'07) received the Ph.D. degree in electrical engineering from Carnegie Mellon University, Pittsburgh, PA, in 1979.

From 1978 to 1981, he was engaged in fiber-optic network component research with GTE Laboratories Inc. In 1981, he joined the Central Research Laboratories, Texas Instruments Incorporated, where he was involved in development of GaAs power field-effect transistors (FETs) and monolithic microwave integrated circuits (MMICs). He has developed a large-signal model of a power FET, dual-gate FETs for gain control, high-power distributed amplifiers, and various millimeter-wave MMICs. In 1989, he joined the Pohang University of Science and Technology (POSTECH), Pohang, Gyeongbuk, Korea, where he is a POSTECH Fellow and a Namko Professor with the Department of Electrical Engineering, and Director of the Microwave Application Research Center, where he is involved in device and circuit technology for RF integrated circuits (RFICs). He has authored over 300 technical papers.

Prof. Kim is a member of the Korean Academy of Science and Technology and the National Academy of Engineering of Korea. He was an associate editor for the IEEE TRANSACTIONS ON MICROWAVE THEORY AND TECHNIQUES, a Distinguished Lecturer of the IEEE Microwave Theory and Techniques Society (IEEE MTT-S), and an Administrative Committee (AdCom) member.